Acta Mechanica 104, 215–230 (1994)

ACTA MECHANICA

Three dimensional numerical and asymptotic solutions for the peristaltic transport of a heat-conducting fluid

D. Tang, Worcester, Massachusetts

(Received September 17, 1992; revised January 25, 1993)

Summary. Using the Oberbeck-Boussinesq (O-B) equations as a mathematical model, asymptotic solutions in closed form and numerical solutions are obtained for the peristaltic transport of a heat-conducting fluid in a three-dimensional flexible tube. The results show that the relation between mass flux and pressure drop remains almost linear and the efficiency of the transport depends mainly on the ratio of the wave amplitude h and the average radius of the tube d. However, the 3-D flow is much different from the 2-D flow in the following ways: (i) The 3-D flow is much more sensitive to the change of the volume expansion coefficient α_T; (ii) Trapping and backflow are much more common in 3-D case; (iii) The longwave asymptotic approximation in 3-D case is not as good as in 2-D case, especially when α_T is not small; (iv) The 3-D flow is more sensitive to Reynolds number change.

1 Introduction and summary of previous results

Peristaltic pumping, the physiological phenomenon of a circumferential progressive wave of contraction or expansion propagating along a flexible tube, plays an essential role in transporting fluid inside living organisms. Many modern mechanical devices have been designed on the principle of peristaltic pumping to transport fluids without internal moving parts, for example, the blood pump in heart-lung machine and peristaltic transport of noxious fluid in nuclear industry. In the latter case, temperature plays a significant role and has to be considered.

The earlier mathematical work on the problem of peristaltic transport was based upon a viscous fluid model governed by the Navier-Stokes equations subject to a prescribed velocity on the boundary of the tube. A review of the research results can be found in the articles by Jaffrin and Shapiro [1] and Winet [2]. Numerical studies of two-dimensional and axisymmetric peristaltic flows can be found in the articles by S. Takabatake, K. Ayukawa and A. Mori [3], [4]. Recently more refined models have been developed to deal with the peristaltic transport of a fluid-particle mixture or a heat-conducting fluid. The former was studied by Hung and Brown [5], Kaimal [6], Fauci [7], and the latter by Bestman [8] and Tang and Shen [9], [10]. In the papers of Tang and Shen [9], [10] the existence and uniqueness of a solution to the O-B equations subject to Newton's cooling law at the boundary were proved, and the asymptotic methods developed for the approximate solution of the O-B equations were justified. The problem was solved over a two-dimensional channel numerically and asymptotically. It is found that: (i) Long-wave expansion is a good approximation to the exact solution; (ii) Temperature has a significant effect on the flow and can cause trapping and back flow; (iii) The relation between mass flux and pressure drop is almost linear.

However, from the physical point of view, it is more practical to consider a three-dimensional tube rather than a two-dimensional channel. In this paper, we intend to solve the problem in an

axisymmetric tube (see Fig. 1). The presence of temperature makes it necessary to solve the problem in three-dimensional setting. The O-B equations are used as the governing equations. It is also assumed that the boundary of the tube is in the form of a sinusoidal travelling wave. Because the stream-vortex function method works for 2-D case only, equations in terms of the primitive variables have to be used. We formulate the problem in Section 2. In Section 3, longwave asymptotic expansion was developed and solutions in closed form were obtained for the zeroth order approximation. In Section 4 an iterated numerical method is presented to solve the exact equations. Then finally, numerical results were presented and discussed in Section 5.

2 Formulation

We consider the peristaltic motion of a heat-conducting fluid in a three-dimensional tube (see Fig. 1) with boundary Γ defined by

$$\Gamma: \quad r = d + h \sin 2\pi(x - ct)/l, \tag{2.1}$$

where $0 < h < d$, h is the wave amplitude, d the average radius of the tube, l the wave length, c the wave velocity. The radial velocity of the tube is given by

$$v_r = dr/dt = -2\pi c(h/l) \cos 2\pi(x - ct)/l. \tag{2.2}$$

We assume that the tube has no horizontal and azimuthal motion. In reference to a coordinate system moving with the travelling wave in the x-direction, the tube becomes stationary, and we further assume that the fluid motion is steady. Using c as measure for velocity, d as unit length, and introducing cylindrical coordinates:

$$x = x,$$

$$y = r \cos \theta,$$

$$z = r \sin \theta,$$

and the cylindrical representation of the velocity field $\boldsymbol{u} = (u, v_r, w_\theta)$ in terms of the Cartesian representation:

$$u = u, \tag{2.3}$$

$$v_r = v \cos \theta + w \sin \theta, \tag{2.4}$$

$$v_\theta = -v \sin \theta + w \cos \theta, \tag{2.5}$$

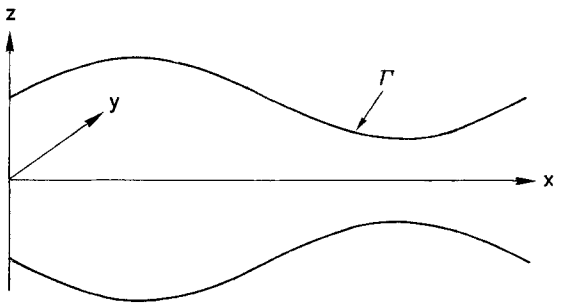

Fig. 1. The flexible tube with its boundaries

the nondimensionalized governing equations [10], [11] are given by

$$u\frac{\partial u}{\partial x}+v_r\frac{\partial u}{\partial r}+\frac{v_\theta}{r}\frac{\partial u}{\partial \theta}=-\frac{\partial p}{\partial x}+\frac{1}{R}\nabla^2 u, \tag{2.6}$$

$$u\frac{\partial v_r}{\partial x}+v_r\frac{\partial v_r}{\partial r}+\frac{v_\theta}{r}\frac{\partial v_r}{\partial \theta}-\frac{(v_\theta)^2}{r}=-\frac{\partial p}{\partial r}+\frac{1}{R}\left(\nabla^2 v_r-\frac{v_r}{r^2}-\frac{2}{r^2}\frac{\partial v_\theta}{\partial \theta}\right)+\alpha_T T\sin\theta, \tag{2.7}$$

$$u\frac{\partial v_\theta}{\partial x}+v_r\frac{\partial v_\theta}{\partial r}+\frac{v_\theta}{r}\frac{\partial v_\theta}{\partial \theta}+\frac{v_\theta v_r}{r}=-\frac{1}{r}\frac{\partial p}{\partial \theta}+\frac{1}{R}\left(\nabla^2 v_\theta+\frac{2}{r^2}\frac{\partial v_r}{\partial \theta}-\frac{v_\theta}{r^2}\right)+\alpha_T T\cos\theta, \tag{2.8}$$

$$\frac{\partial u}{\partial x}+\frac{v_r}{r}+\frac{\partial v_r}{\partial r}+\frac{1}{r}\frac{\partial v_\theta}{\partial \theta}=0, \tag{2.9}$$

$$u\frac{\partial T}{\partial x}+v_r\frac{\partial T}{\partial r}+\frac{v_\theta}{r}\frac{\partial T}{\partial \theta}=P_e{}^{-1}\nabla^2 T+Q_T, \tag{2.10}$$

$$\Gamma:\quad r_+=1+a\sin 2\pi\alpha x, \tag{2.11}$$

$$(u, v_r, v_\theta)|_\Gamma=(-1, -2\pi a\alpha\cos 2\pi\alpha x, 0), \tag{2.12}$$

$$\left(P_e{}^{-1}\frac{\partial T}{\partial n}+h_T T\right)\Big|_\Gamma=\varphi, \tag{2.13}$$

$$p(l, y, z)-p(0, y, z)=p_d. \tag{2.14}$$

Q_T, φ are prescribed functions which are periodic in x with period $l=1/\alpha$, $a=h/d$ is the amplitude/radius ratio, R is the Reynolds number, $P_e{}^{-1}$ is the Peclet number, h_T is a heat conducting coefficient, α_T is the constant volume expansion coefficient, p_d is the prescribed pressure-drop, and

$$\nabla^2=\frac{\partial^2}{\partial x^2}+\frac{\partial^2}{\partial r^2}+\frac{1}{r}\frac{\partial}{\partial r}+\frac{1}{r^2}\frac{\partial^2}{\partial \theta^2}. \tag{2.15}$$

To facilitate numerical computations, we finally map the domain to a rectangular block by the transformation

$$\xi=x,\quad \eta=r/[1+a\sin 2\pi\alpha x],\quad \theta=\theta. \tag{2.16}$$

Equation (2.16) transforms $\{(x, r, \theta)\,|\,0\leqq x\leqq 1/\alpha,\ 0\leqq r\leqq 1+a\sin 2\pi\alpha x,\ 0\leqq\theta\leqq 2\pi\}$ to $\{(\xi, \eta, \theta)\,|\,0\leqq\xi\leqq 1/\alpha,\ 0\leqq\eta\leqq 1,\ 0\leqq\theta\leqq 2\pi\}$. Using the following formulae:

$$f_x=f_\xi+f_\eta\eta_x,\quad f_r=f_\eta\eta_r,$$

$$f_{xx}=f_{\xi\xi}+2f_{\xi\eta}\eta_x+f_{\eta\eta}\eta_x{}^2+f_\eta\eta_{xx},\quad f_{rr}=f_{\eta\eta}\eta_r{}^2,$$

$$f_{xx}+f_{rr}=f_{\xi\xi}+2f_{\xi\eta}\eta_x+f_{\eta\eta}(\eta_x{}^2+\eta_r{}^2)+f_\eta\eta_{xx},$$

the system can be rewritten in terms of (ξ, η, θ) and is solved numerically in Section 4.

3 Longwave asymptotic expansion

In this Section we will try to find the longwave solutions in closed form using the techniques developed by Bestman [8] and Tang and Shen [10]. A closed form solution will enable us to see the flow properties clearly. It can also be used as the numerical initial condition to gain fast convergence. We introduce the notation

$$(u, v_r, v_\theta) = (u^* - 1, v, w),$$

and then drop the * for convenience. We also prescribe the flux condition [10] instead of the pressure drop condition. The system becomes

$$-u_x + uu_x + vu_r + \frac{w}{r} u_\theta = -p_x + \frac{1}{R} \nabla^2 u,$$

$$-v_x + uv_x + vv_r + \frac{w}{r} v_\theta - \frac{w^2}{r} = -p_r + \frac{1}{R}\left(\nabla^2 v - \frac{v}{r^2} - \frac{2}{r^2} w_\theta\right) + \alpha_T T \sin\theta,$$

$$-w_x + uw_x + vv_r + \frac{w}{r} w_\theta + \frac{vw}{r} = -\frac{1}{r} p_\theta + \frac{1}{R}\left(\nabla^2 w + \frac{2}{r^2} v_\theta - \frac{w}{r^2}\right) + \alpha_T T \cos\theta,$$

$$u_x + \frac{v}{r} + v_r + \frac{1}{r} w_\theta = 0,$$

$$-T_x + uT_x + vT_r + \frac{w}{r} T_\theta = P_e^{-1} \nabla^2 T + Q_T, \tag{3.1}$$

$$\Gamma: \quad r_+ = 1 + a \sin 2\pi\alpha x,$$

$$(u, v_r, v_\theta)|_\Gamma = (0, -2\pi a\alpha \cos 2\pi\alpha x, 0),$$

$$\left(P_e^{-1} \frac{\partial T}{\partial n} + h_T T\right)\Big|_\Gamma = \varphi,$$

$$\int_0^{r_+} \int_0^{2\pi} (u - 1)\, r\, dr\, d\theta = Q_f$$

where the subscripts by x, r, θ indicate partial derivatives and Q_f is the prescribed flux. Noting that along the tube

$$\bar{U} = (u - 1, v_r, v_\theta) = (-1, -2\pi a\alpha \cos 2\pi\alpha x, 0),$$

and that the normal direction of Γ in cylindrical coordinates is given by

$$\boldsymbol{n} = (n_x, n_r, n_\theta) = (-2\pi a\alpha \cos 2\pi\alpha x, 1, 0),$$

we have:

$$\bar{U} \cdot \boldsymbol{n}|_\Gamma = 0.$$

We apply the divergence theorem to the integral

$$0 = \int_{\Omega^*} \nabla \cdot \bar{U}\, dV = \int_{\Gamma_1} \bar{U} \cdot \boldsymbol{n}\, dS + \int_{\Gamma_2} \bar{U} \cdot \boldsymbol{n}\, dS + \int_{\Gamma_3} \bar{U} \cdot \boldsymbol{n}\, dS$$

$$= -\int_{\Gamma_1} (u - 1)\, dS + \int_{\Gamma_3} (u - 1)\, dS,$$

where Γ_i is the cross section of the tube at $x = x_i, i = 1, 3$ respectively, Γ_2 is the tube lateral surface between the two cross sections and Ω^* is the volume bounded by these surfaces. From here, it is clear that

$$\int_{\Gamma_1} (u - 1)\, dS = \int_{\Gamma_3} (u - 1)\, dS,$$

i.e., Q_f in (3.1) is a constant. To introduce the longwave asymptotic scheme, we make the following assumptions:

$$\alpha = d/l \ll 1, \quad v = O(\alpha), \quad w = O(\alpha), \quad R = O(\alpha), \quad P_e = O(\alpha), \quad h_T = O(1/\alpha), \quad p = O(\alpha^{-2}).$$

Using * to indicate the new variables, we have

$$(\alpha x, r, \theta) = (x^*, r, \theta), \quad (u, v, w) = (u^*, \alpha v^*, \alpha w^*), \quad \partial/\partial x = \alpha\, \partial/\partial x^*,$$

$$R = \alpha R^*, \quad P_e^{-1} = k_T^*/\alpha, \quad h_T = h_T^*/\alpha, \quad Q_T = Q_T^*/\alpha, \quad \varphi = \varphi^*/\alpha, \quad p = p^*/(\alpha^2).$$

We substitute these into (3.1) and drop all the *'s,

$$\alpha^2 \left(-u_x + uu_x + vu_r + \frac{w}{r} u_\theta\right) = -p_x + \frac{1}{R} (\alpha^2 u_{xx} + \nabla_2^2 u), \tag{3.2.1}$$

$$\alpha^3 \left(-v_x + uv_x + vv_r + \frac{w}{r} v_\theta - \frac{w^2}{r}\right) = -\frac{p_r}{\alpha} + \frac{1}{R}\left(\alpha^3 v_{xx} + \alpha\left(\nabla_2^2 v - \frac{v}{r^2} - \frac{2}{r^2} w_\theta\right)\right) + \alpha_T T \sin\theta, \tag{3.2.2}$$

$$\alpha^3 \left(-w_x + uw_x + vv_r + \frac{w}{r} w_\theta + \frac{vw}{r}\right) = -\frac{1}{r} p_\theta + \frac{1}{R}\left(\alpha^3 w_{xx} + \alpha\left(\nabla_2^2 w + \frac{2}{r^2} v_\theta - \frac{w}{r^2}\right)\right) + \alpha_T T \cos\theta, \tag{3.2.3}$$

$$u_x + \frac{v}{r} + v_r + \frac{1}{r} w_\theta = 0, \tag{3.2.4}$$

$$a^2 \left(-T_x + uT_x + vT_r + \frac{w}{r} T_\theta\right) = P_e^{-1}(\alpha^2 T_{xx} + \nabla_2^2 T) + Q_T, \tag{3.2.5}$$

$$\Gamma: \quad r_+ = 1 + a \sin 2\pi x, \tag{3.2.6}$$

$$(u, v_r, v_\theta)|_\Gamma = (0, -2\pi a \cos 2\pi x, 0), \tag{3.2.7}$$

$$\left(P_e^{-1} \frac{-2\pi a \alpha^2 (\cos 2\pi x)\, T_x + T_r}{(1 + (2\pi a \alpha \cos 2\pi x)^2)^{1/2}} + h_T T\right)\Big|_\Gamma = \varphi, \tag{3.2.8}$$

$$\int_0^{r_+} \int_0^{2\pi} (u - 1)\, r\, dr\, d\theta = Q_f, \tag{3.2.9}$$

where

$$\nabla_2^2 = \frac{\partial^2}{\partial r^2} + \frac{1}{r}\frac{\partial}{\partial r} + \frac{1}{r^2}\frac{\partial^2}{\partial \theta^2}.$$

The equations for the zeroth order approximation are

$$\frac{1}{R}\nabla_2^2 u_0 = p_{0x},$$

$$p_{0r} = 0,$$

$$p_{0\theta} = 0,$$

$$u_0|_\Gamma = 0, \tag{3.3}$$

$$\int_0^{r_+}\int_0^{2\pi} (u_0 - 1)\, r\, dr\, d\theta = Q_f,$$

$$P_e^{-1}\nabla_2^2 T_0 = -Q_T,$$

$$(P_e^{-1}T_0 + h_T T_0)|_\Gamma = \varphi.$$

u_0, T_0 and p_0 can be solved from here. For simplicity, assuming Q_T and φ to be constants, we get

$$u_0 = \left(\frac{2Q_f}{\pi r_+^2} + 2\right)\left(1 - \frac{r^2}{r_+^2}\right). \tag{3.4}$$

$$p_0 = -\frac{8Q_f}{R\pi}\int_0^x r_+^{-4}\, dx - \frac{8}{R}\int_0^x r_+^{-2}\, dx + p_0(0). \tag{3.5}$$

$$T_0 = \frac{\varphi}{h_T} + \frac{Q_T}{2h_T} r_+ + \frac{1}{4}\frac{Q_T}{k_T}(r_+^2 - r^2), \tag{3.6}$$

where

$$r_+ = 1 + a\sin 2\pi x. \tag{3.7}$$

In the following we will try to determine v_0 and w_0. Eliminating p from the first two equations of (3.2) by cross differentiation, comparing the $O(\alpha)$ terms and using the identities

$$\frac{\partial}{\partial r}(r\nabla_2^2 w_0) - \frac{w_{0r}}{r} + \frac{w_0}{r^2} + \frac{2w_{0\theta\theta}}{r^2} = r\nabla_2^2\left(\frac{1}{r}\frac{\partial}{\partial r}(rw_0)\right), \tag{3.8}$$

$$\nabla_2^2 v_{0\theta} - \frac{2v_{0r\theta}}{r} + \frac{v_{0\theta}}{r^2} = r\nabla_2^2\left(\frac{1}{r}\frac{\partial}{\partial\theta}(v_0)\right), \tag{3.9}$$

we come up with

$$\frac{1}{R}\left(\nabla_2^2\left(\frac{1}{r}\frac{\partial}{\partial r}(rw_0)\right) - \nabla_2^2\left(\frac{1}{r}\frac{\partial}{\partial\theta}(v_0)\right)\right) + \alpha_T T_{0r}\cos\theta = 0. \tag{3.10}$$

From the (3.2.3) we have

$$u_{0x} + \frac{v_0}{r} + v_{0r} + \frac{1}{r}w_{0\theta} = 0. \tag{3.11}$$

The boundary conditions for v_0 and w_0 are

$$(v_0, w_0) = (-2\pi a\cos 2\pi x, 0) = (-r_+', 0), \tag{3.12}$$

where the prime ′ indicates the derivative with respect to x. Let

$$v_0 = g_0(x, r) \sin\theta - \frac{R}{16} p_0'' r^3 - \frac{R}{2} B_0' r, \tag{3.13}$$

$$w_0 = h_0(x, r) \cos\theta, \tag{3.14}$$

where g_0 and h_0 are to be determined and satisfy

$$g_0(x, r_+) = 0, \quad h_0(x, r_+) = 0. \tag{3.15}$$

It can be checked easily that the boundary conditions for v_0 and w_0 are satisfied. Using (3.10)–(3.15) and the techniques in [8], going through some tedious manipulations, we obtain

$$g_0 = -\frac{P_e R \alpha_T Q_T}{384} [r^2 - r_+^2]^2, \tag{3.16}$$

$$h_0 = -\frac{P_e R \alpha_T Q_T}{384} (5r^2 - r_+^2)(r^2 - r_+^2). \tag{3.17}$$

Therefore,

$$v_0 = -\frac{P_e R \alpha_T Q_T}{384} [r^2 - r_+^2]^2 \sin\theta - \frac{R}{16} p_0'' r^3 - \frac{R}{2} B_0' r, \tag{3.18}$$

$$w_0 = -\frac{P_e R \alpha_T Q_T}{384} (5r^2 - r_+^2)(r^2 - r_+^2) \cos\theta, \tag{3.19}$$

where

$$p_0''(x) = \left(\frac{32 Q_f}{R\pi r_+^5} + \frac{16}{R r_+^3}\right) r_+',$$

$$B_0'(x) = -\frac{4 Q_f}{R\pi r_+^3} r_+',$$

and again the prime ′ indicates the derivative with respect to x.

Back to the original parameters and quantities used in Section 2, we have the zeroth order longwave approximation to the solution of the system (2.6)–(2.14):

$$u_0 = \left(\frac{2Q_f}{\pi r_+^2} + 2\right)\left(1 - \frac{r^2}{r_+^2}\right) - 1, \tag{3.20}$$

$$v_0 = -\frac{R \alpha_T Q_T}{384 k_T} [r^2 - r_+^2]^2 \sin\theta - \left(\frac{2Q_f}{\pi r_+^5} + \frac{1}{r_+^3}\right) r_+' r^3 + \frac{2Q_f}{\pi r_+^3} r_+' r, \tag{3.21}$$

$$w_0 = -\frac{R \alpha_T Q_T}{384 k_T} (5r^2 - r_+^2)(r^2 - r_+^2) \cos\theta, \tag{3.22}$$

$$p_0 = -\frac{8 Q_f}{R\pi} \int_0^x r_+^{-4}\, dx - \frac{8}{R} \int_0^x r_+^{-2}\, dx + p_0(0), \tag{3.23}$$

$$T_0 = \frac{\varphi}{h_T} + \frac{Q_T}{2h_T} r_+ + \frac{1}{4}\frac{Q_T}{k_T}(r_+{}^2 - r^2). \tag{3.24}$$

$$p_d = -\frac{8Q_f}{R\pi}\int_0^l r_+{}^{-4}\,dx - \frac{8}{R}\int_0^l r_+{}^{-2}\,dx. \tag{3.25}$$

These solutions are used as numerical initial condition in the numerical computations.

4 Numerical method for the exact equations

We use the regularized central difference scheme and the extended successive-over-relaxation (E.S.O.R) iterative method suggested by Strikwerda [12], [13] to solve the system (2.6)–(2.14). The finite difference scheme used here is briefly explained below. Let d_1, d_2 and d_3 be the spans of finite differences for ξ, η, θ, respectively. The following formulas were used for the derivatives to convert the differential equations into finite difference equations:

$$f(i,j,k) = f(\xi_i, \eta_j, \theta_k) = f(i\cdot d_1, j\cdot d_2, k\cdot d_3),$$

$$f_{\xi\xi}(i,j,k) = [f(i+1,j,k) + f(i-1,j,k) - 2f(i,j,k)]/d_1{}^2,$$

$$f_{\eta\eta}(i,j,k) = [f(i,j+1,k) + f(i,j-1,k) - 2f(i,j,k)]/d_2{}^2.$$

$$f_{\theta\theta}(i,j,k) = [f(i,j,k+1) + f(i,j,k-1) - 2f(i,j,k)]/d_3{}^2.$$

$$f_{\xi\eta}(i,j,k) = [f(i+1,j+1,k) - f(i-1,j+1,k) - f(i+1,j-1,k) + f(i-1,j-1,k)]/(4d_1d_2),$$

$$f_{\xi}(i,j,k) = \delta_{\xi\circ} f - (1/6)\, d_1{}^2\delta_{\xi-}\delta_{\xi+}^2 f,$$

$$f_{\eta}(i,j,k) = \delta_{\eta\circ} f - (1/6)\, d_2{}^2\delta_{\eta-}\delta_{\eta+}^2 f,$$

$$f_{\theta}(i,j,k) = \delta_{\theta\circ} f - (1/6)\, d_3{}^2\delta_{\theta-}\delta_{\theta+}^2 f,$$

where

$$(\delta_{\xi\circ} f)\,(i,j,k) = [f(i+1,j,k) - f(i-1,j,k)]/(2d_1),$$

$$(\delta_{\xi+} f)\,(i,j,k) = [f(i+1,j,k) - f(i,j,k)]/d_1,$$

$$(\delta_{\xi-} f)\,(i,j,k) = [f(i,j,k) - f(i-1,j,k)]/d_1,$$

and the corresponding differences for η and θ can be defined similarly. The iterative scheme is given below:

$$\begin{aligned} u^*(i,j,k) = u(i,j,k) - \omega \Bigg\{ & u(i,j,k) \\ & - \Bigg[r^2 \left(\frac{u(i+1,j,k) + u(i-1,j,k)}{d_1{}^2} + \frac{u(i,j+1,k) + u(i,j-1,k)}{d_2{}^2}(\eta_x{}^2 + \eta_r{}^2) \right) \\ & + \frac{u(i,j,k+1) + u(i,j,k-1)}{d_3{}^2} + r^2(2u_{\xi\eta}\eta_x + u_\eta \eta_{xx}) \\ & - Rr^2(u(u_\xi + u_\eta\eta_x) + vu_\eta\eta_r) - Rrwu_\theta - Rr^2(p_\xi + p_\eta\eta_x) + ru_\eta\eta_r \Bigg] \Bigg/ \\ & \left[r^2 \left(\frac{2}{d_1{}^2} + \frac{2}{d_2{}^2}(\eta_x{}^2 + \eta_r{}^2) \right) + \frac{2}{d_3{}^2} \right] \Bigg\}, \end{aligned} \tag{4.1}$$

$$v^*(i,j,k) = v(i,j,k) - \omega \Big\{ v(i,j,k) \Big[r^2 \left(\frac{v(i+1,j,k) + v(i-1,j,k)}{{d_1}^2} + \frac{v(i,j+1,k) + v(i,j-1,k)}{{d_2}^2} ({\eta_x}^2 + {\eta_r}^2) \right) + \frac{v(i,j,k+1) + v(i,j,k-1)}{{d_3}^2} + r^2(2v_{\xi\eta}\eta_x + v_\eta \eta_{xx}) - Rr^2\big(u(v_\xi + v_\eta \eta_x) + v v_\eta \eta_r + p_\eta \eta_r - \alpha_T T \sin\theta\big) - Rr(wv_\theta - w^2) + r v_\eta \eta_r - 2w_\theta \Big] \Big/ \Big[r^2 \left(\frac{2}{{d_1}^2} + \frac{2}{{d_2}^2} ({\eta_x}^2 + {\eta_r}^2) \right) + \frac{2}{{d_3}^2} + 1 \Big] \Big\}, \tag{4.2}$$

$$w^*(i,j,k) = w(i,j,k) - \omega \Big\{ w(i,j,k) - \Big[r^2 \left(\frac{w(i+1,j,k) + w(i-1,j,k)}{{d_1}^2} + \frac{w(i,j+1,k) + w(i,j-1,k)}{{d_2}^2} ({\eta_x}^2 + {\eta_r}^2) \right) + \frac{w(i,j,k+1) + w(i,j,k-1)}{{d_3}^2} + r^2(2w_{\xi\eta}\eta_x + w_\eta \eta_{xx}) - Rr^2\big(u(w_\xi + w_\eta \eta_x) + v w_\eta \eta_r - \alpha_T T \cos\theta\big) - Rr(ww_\theta + wv + p_\theta) + r w_\eta \eta_r + 2v_\theta \Big] \Big/ \Big[r^2 \left(\frac{2}{{d_1}^2} + \frac{2}{{d_2}^2} ({\eta_x}^2 + {\eta_r}^2) \right) + \frac{2}{{d_3}^2} + 1 \Big] \Big\}, \tag{4.3}$$

$$T^*(i,j,k) = T(i,j,k) - \omega \Big\{ T(i,j,k) - \Big[r^2 \left(\frac{T(i+1,j,k) + T(i-1,j,k)}{{d_1}^2} + \frac{T(i,j+1,k) + T(i,j-1,k)}{{d_2}^2} ({\eta_x}^2 + {\eta_r}^2) \right) + \frac{T(i,j,k+1) + T(i,j,k-1)}{{d_3}^2} + r^2(2T_{\xi\eta}\eta_x + T_\eta \eta_{xx}) - r^2\big(u(T_\xi + T_\eta \eta_x) + v T_\eta \eta_r\big)/{P_e}^{-1} - r w T_\theta / {P_e}^{-1} + r^2 Q_T / {P_e}^{-1} + r T_\eta \eta_r \Big] \Big/ \Big[r^2 \left(\frac{2}{{d_1}^2} + \frac{2}{{d_2}^2} ({\eta_x}^2 + {\eta_r}^2) \right) + \frac{2}{{d_3}^2} \Big] \Big\}, \tag{4.4}$$

$$p^*(i,j,k) = p(i,j,k) - \gamma\{[r(u_\xi + u_\eta \eta_x) + v + r v_\eta \eta_r + w_\theta] - \delta\}, \tag{4.5}$$

where u^*, v^*, w^*, T^* and p^* are the updated values of the corresponding functions, ω and γ are iteration constants. Note according to Strikwerda, instead of satisfying the equation

$$\nabla \cdot \boldsymbol{u} = 0,$$

we use

$$\nabla \cdot \boldsymbol{u} = \delta, \tag{4.6}$$

where δ is the average of $\nabla \cdot \boldsymbol{u}$ and is of the order of truncation error after some iterations. This improves convergence.

The values inside $\{\cdots\}$ of (4.1)–(4.5) are actually the imbalances of the corresponding equations and are used as the measurements of the errors of the computations.

For the boundary conditions in ξ-direction, we impose periodic conditions for u, v, w and T and the pressure drop condition for p:

$$p(l, \eta, \theta) = p(0, \eta, \theta) + p_d.$$

At $\eta = 1$, cubic interpolation was used for pressure, and boundary conditions (2.12)–(2.13) were used for (u, v, w) and T. Periodic conditions were imposed for all functions at $\theta = 0, 2\pi$.

Due to the singularity of the polar coordinate system, special arrangement has to be made for the boundary conditions at $\eta = 0$ [14]. For the pressure and temperature, we take averages of the function values around the ξ-axis (i.e., $\eta = 0$) and then use cubic extrapolation for the function values at $\eta = 0$. In terms of formulas, let

$$f_1(i) = \sum_{k=0}^{n-1} f(i, 1, k)/n,$$

$$f_2(i) = \sum_{k=0}^{n-1} f(i, 2, k)/n,$$

then the function values at $\eta = 0$ are given by

$$f(i, 0, k) = (4 \cdot f_1(i) - f_2(i))/3, \quad k = 0, \ldots, n.$$

The polar coordinate representation of the velocity field is multivalued at $\eta = 0$. Let (V, W) be the Cartesian representation, then the relation between (V, W) and the polar notation (v, w) is given below:

$$v = V \cos\theta + W \sin\theta,$$

$$w = -V \sin\theta + W \cos\theta.$$

To determine the values of (v, w) at $\eta = 0$, we first compute the Cartesian velocity (V, W) at $j = 1, 2$, the neighborhood around $j = 0$. Then in the same way as we did for the scalar function, we find the values $(V_0(i), W_0(i))$ of (V, W) at $\eta = 0$ (note: (V, W) is single valued). Now the values of (v, w) can be calculated from

$$v(i, 0, k) = V_0(i) \cos\theta_k + W_0(i) \sin\theta_k,$$

$$w(i, 0, k) = -V_0(i) \sin\theta_k + W_0(i) \cos\theta_k,$$

where $\theta_k = (2\pi k)/n$.

Our experience indicates that $\omega = 0.1 - 1.0$ and $\gamma = 0.1 - 0.01$ give good convergence. Computations were carried out for various situations and results are given in Section 5.

5 Results of the computations and discussions

We are interested in the accuracy of the longwave approximation, the flux-pressure drop relations, the efficiency of the transport and the influences of various parameters on the flow. Special attention was paid to observe differences between the results from the 3-D model and the

results from the 2-D model. To show the 3-D solution, different cross-sections were taken to observe the details of the flow. As an example, Fig. 2 gives θ-cross sections of the $u - v$ velocity field, the pressure and temperature field at $\theta = 0°$ and 90°, x-cross sections of the $v - w$ field at $x = 0, l/4, l/2$ and $3l/4$. In the $u - v$ direction field, darker lines indicate positive flow where flow goes faster than the wave speed. When drawing the pressure and temperature fields, a cross "X"

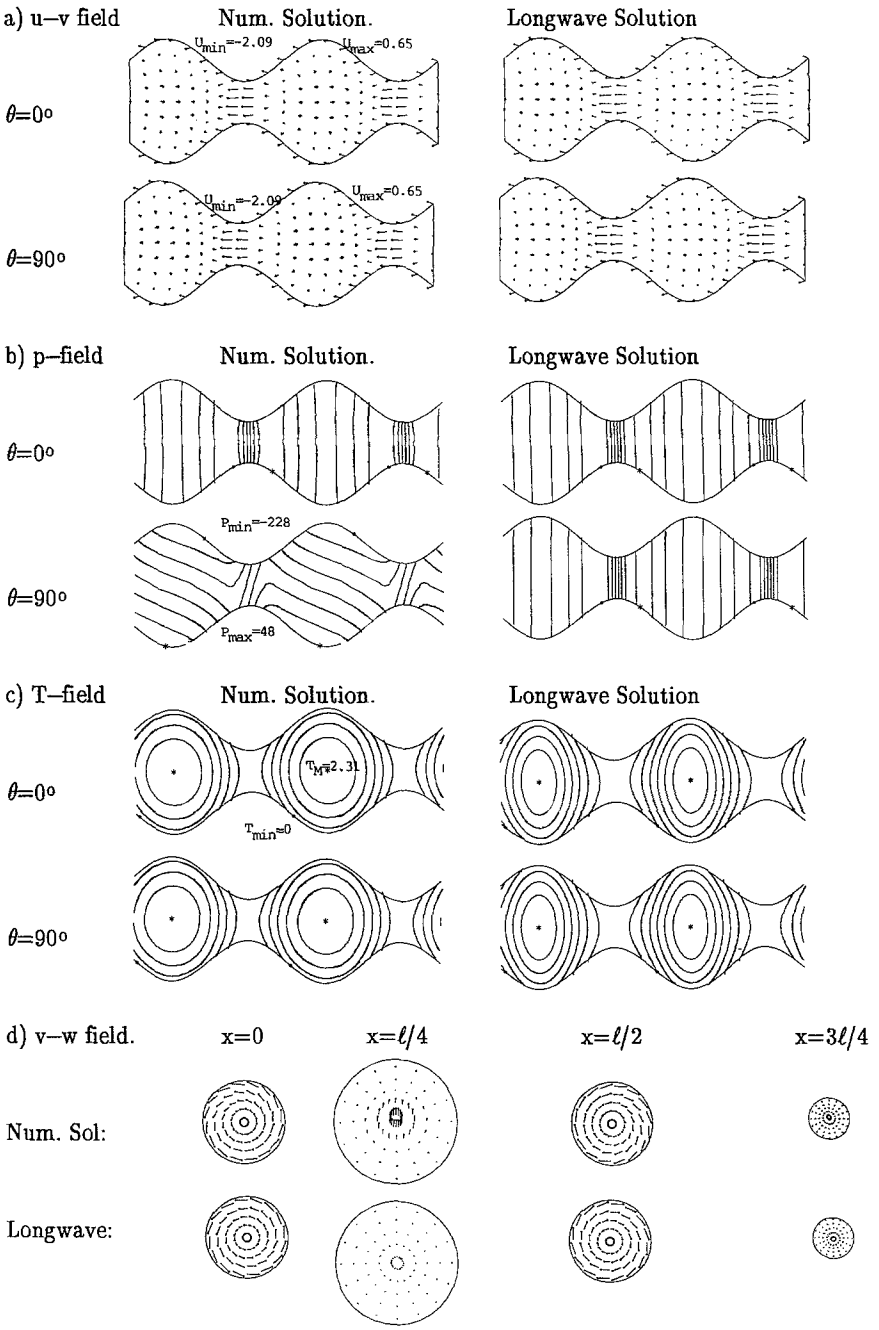

Fig. 2. Velocity, pressure and temperature field of solutions $R = 0.1$, $P_e = 0.1$, $h_T = 10$, $\alpha_T = 100$, $Q_T = 10$, $\varphi = 10$, $P_d = -1$, $\alpha = 0.1$, $a = 0.5$

indicates where the field gets maximum and a dot "·" indicates minimum. By studying the solutions, we have the following observations:

(i) Accuracy of the longwave approximation

From Table 1 we see that the longwave solutions provide good approximations to the exact solutions, especially for u, T and p. The approximations for v and w were not as good. The reason for this is that the assumptions $v = O(\alpha)$ and $w = O(\alpha)$ are not true when α_T is not small. Table 2 shows that the relative errors for v and w can be as high as 23% when $\alpha_T = 100$ and $\alpha = 0.1$. Figure 2 shows clear differences between longwave and numerical solutions.

(ii) Velocity field: positive motion, trappings and backflow

Our results show that backflow and trappings are much more common in 3-D case than in 2-D case. It is common in 3-D case to have backflow at the narrower part of the tube (neck) and a part

Table 1. Comparison between the longwave and the numerical solutions $R = 0.1, P_e = 0.1, h_T = 10, \alpha_T = 10, Q_T = 10, \varphi = 10, P_d = -1, a = 0.5$

α	u	v	w	T	p
Longwave solution relative imbalance					
0.025	0.0000528	0.016166	0.025201	0.0000084	0.00000004
0.05	0.0001951	0.009964	0.017561	0.0000323	0.00000012
0.1	0.0007167	0.006192	0.011763	0.0001194	0.00000034
Numerical solution relative imbalance					
0.025	0.0000002	0.000015	0.000033	0.0000001	0.00000105
0.05	0.0000011	0.000009	0.000021	0.0000004	0.00000163
0.1	0.0000057	0.000006	0.000013	0.0000012	0.00000459
Relative errors of longwave solution compared to numerical solutions					
0.025	0.0061613	0.034728	0.052036	0.0057435	0.00236776
0.05	0.0183438	0.026451	0.039928	0.0197051	0.00337550
0.1	0.0586278	0.041004	0.029868	0.0557106	0.00509389

Note: (i) Longwave solutions give good approximation in general
(ii) When α becomes smaller, the approximation becomes better for u, p, T as expected; the approximations for v and w did not improve because the assumptions $v = O(\alpha)$ and $w = O(\alpha)$ are not true when α_T is not smal.

Table 2. Errors of α_T computations $R = 0.1, P_e = 0.1, h_T = 10, Q_T = 10, \varphi = 10, P_d = -1, \alpha = 0.1, a = 0.5$

α_T	u	v	w	T	p
Long wave relative imbalance					
0	0.0007167	0.002817	0.000000	0.0001194	0.00000023
10	0.0007167	0.006192	0.011763	0.0001194	0.00000048
100	0.0007167	0.055204	0.115071	0.0001194	0.00000342
Numerical solution relative imbalance					
0	0.0000025	0.000002	0.000003	0.0000001	0.00000227
10	0.0000057	0.000006	0.000013	0.0000012	0.00000459
100	0.0000059	0.000045	0.000097	0.0000013	0.00001216
Relative errors of longwave solution compared to numerical solutions					
0	0.0586821	0.033668	0.001595	0.0563730	0.00221658
10	0.0586278	0.041004	0.029868	0.0557106	0.00509389
100	0.0658887	0.138638	0.235067	0.0556214	0.00432304

of positive motion at the wider part of the tube. Trapping then occurs between the positive motion and the boundary. This is because the cross area of the 3-D tube is proportional to the *square of the radius* while the cross "area" of the 2-D channel is linearly proportional to the width of the channel. That makes the pushing in 3-D case much harder when the tube contracts. The fact that backflow appears at the narrower part of the tube indicates that the fluid is leaking backwards there. The positive motion part is twisted when α_T is not small due to buoyant effect. The twisting is more noticeable when α_T is larger.

(iii) Pressure field

The contour lines of the pressure fields are shown in Figs. 2 and 3. The figures show that the maximum of pressure appears at the right side of the "neck" and the minimum appears at the left side of the neck. So the pressure increases when passing the neck and decreases when going through the wider part of the tube. When α_T becomes large, the pressure fields becomes twisted. The maximum appears at the lower part of the tube and the minimum appears at the upper part of the tube. The pressure then pushes the fluid upwards. This agrees with the velocity field.

(iv) Influence of α_T on the solutions

Figure 3 shows the $u - v$ cross sections and pressure field for various α_T values. When $\alpha_T = 0$, there is no buoyant effect. Therefore, the flow is axisymmetric. When α_T becomes larger, the buoyant effect becomes more apparent and the vertical motion becomes more noticeable.

Figure 4 gives 2-D velocity fields for comparison. At $\alpha_T = 100$, the flow is almost symmetric. Even at $\alpha_T = 999$, the buoyant effect is still very small. It takes a much smaller change of α_T to

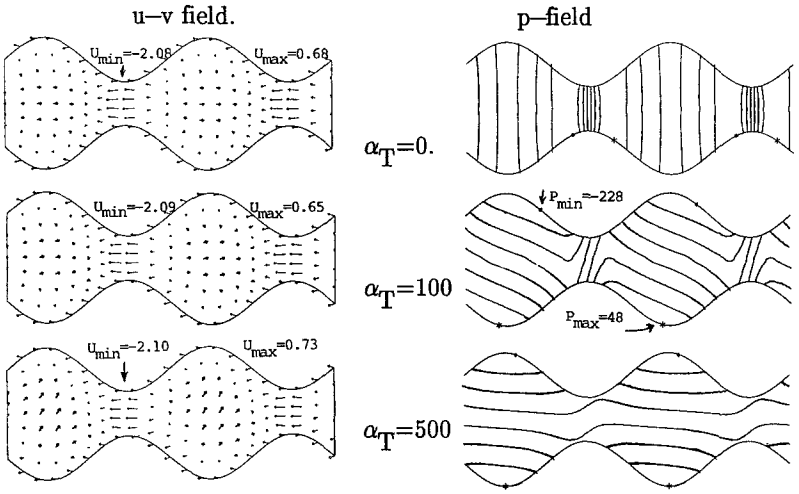

Fig. 3. $u - v$ field and p field with α_T change. $\theta = 90°$, $R = 0.1$, $P_e = 0.1$, $h_T = 10$, $Q_T = 10$, $\varphi = 10$, $P_d = -1$, $\alpha = 0.1$, $a = 0.5$

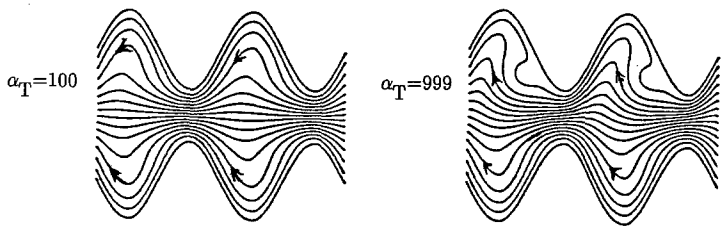

Fig. 4. Two dimensional $u - v$ field with α_T change

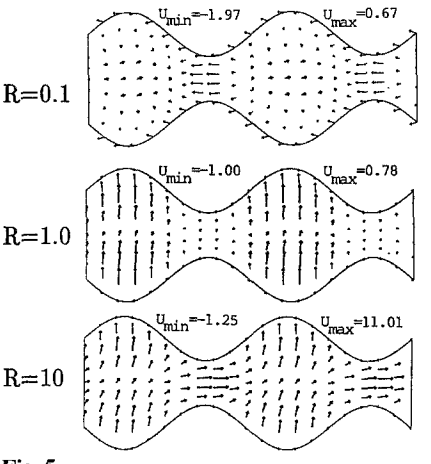

Fig. 5.

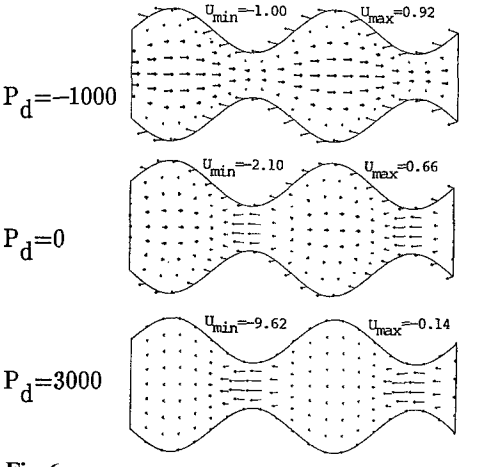

Fig. 6.

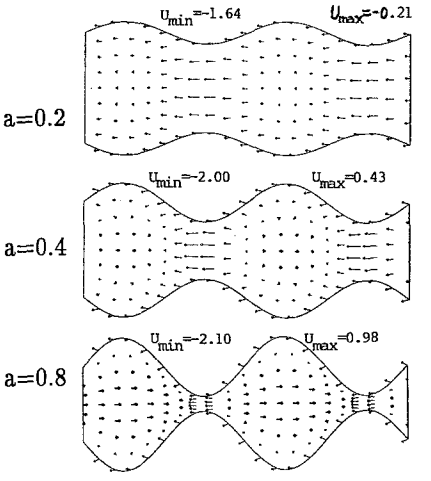

Fig. 7.

Fig. 5. $u - v$ field with R change. $\theta = 90°$, $P_e = \alpha = 0.1$, $\alpha_T = Q_T = \varphi = 10$, $P_d = -50$, $a = 0.5$. *Fig.* 6. $u - v$ field with P_d change. $\theta = 90°$, $R = P_e = \alpha = 0.1$, $h_T = Q_T = \varphi = \alpha_T = 10$, $a = 0.5$. *Fig.* 7. $u - v$ field with $a = h/d$ change. $\theta = 90°$, $R = \alpha = P_e = 0.1$, $h_T = \alpha_T = Q_T = 10$, $P_d = -1$

show a considerable change in the flow in 3-D case. Therefore, temperature is a much more important factor than we might have guessed based on the knowledge from 2-D channel flow.

(v) Influence of Reynolds number on the flow

Figure 5 shows that the solution is sensitive to the changes of Reynolds number. From the figure, we can see that when $R = 0.1$, there is backflow at the neck. However, when $R = 10$, there is no backflow at all. This is because when the fluid is thinner (i.e., R is larger), the pressure is able to push the fluid forward all the way through. We also note that the flow in the vertical direction becomes more noticeable when the Reynolds number becomes larger. The v, w components are no longer small. The reason is the same: when the fluid becomes thinner, the buoyant force causes more noticeable motion in the vertical direction. This also explains why the longwave approximation becomes poorer for larger R values. Numerically, smaller iterative parameters ω and γ should be chosen to compute for larger R values.

(vi) Influence of pressure drop on the flow

Pressure drop is the main driving force of the flow. Figure 6 shows that when the pressure decreases more over the path, it pushes the flow harder, the positive portion becomes larger and more fluid is pushed forward.

(vii) Influence of a-change on the flow

Figure 7 gives the velocity fields with respect to the moving frame for $a = 0.2, 0.4$ and 0.8 where $a = h/d$ is the wave amplitude/tube radius ratio. When a is small, there is no positive flow, no trapping. When a increases, gradually, a small positive flow region appears near the center of the tube. When a becomes larger, the positive flow region becomes larger. a is the main parameter which has major influence on the flux, i.e., the efficiency of the fluid transport. When physically possible, the larger a is, the more efficient the transport will be. But when a is too large (i.e., very close to 1.0. a has to be less than 1.0), the tube may not be able to bear the stretching. So consideration must be given to both the efficiency and the elastic property of the tube. The flux vs. a curve is given in Fig. 8.

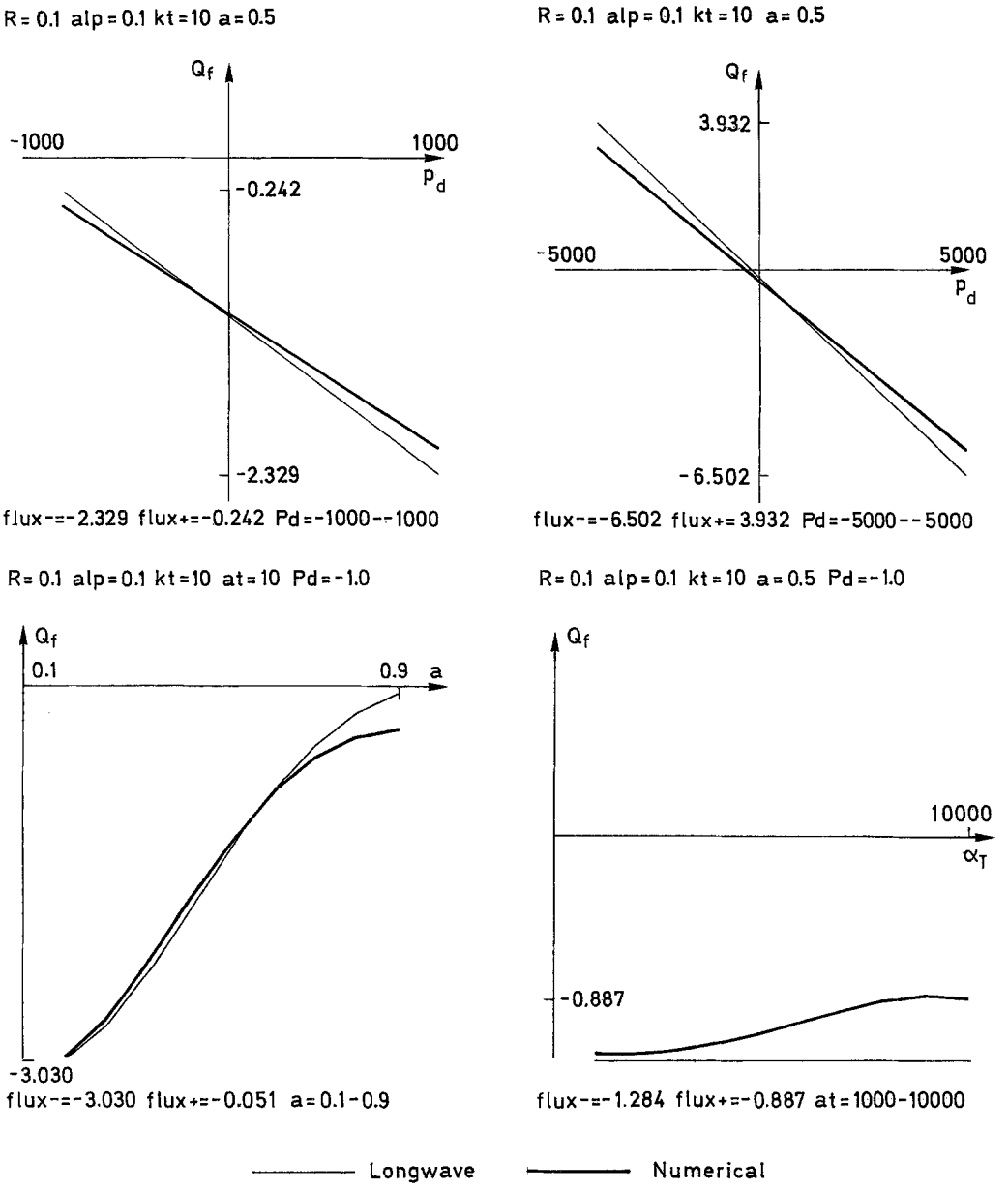

Fig. 8. Flux curves with P_d, α_T and $a = h/d$ changing

(viii) Flux curves

Figure 8 gives $Q_f - p_d$, $Q_f - a$ and $Q_f - \alpha_T$ curves. The $Q_f - p_d$ curve is almost linear. The $Q - a$ curve (flux-wave amplitude) shows when $0.1 \leqq a \leqq 0.6$, the relation is almost linear. When $0.6 < a$, the increase becomes slower. It seems $0.6 \leqq a \leqq 0.7$ is a good region to gain good efficiency without requiring extreme stretching of the tube. The $Q_T - \alpha_T$ curve shows that flux increases with α_T and then the curve becomes almost flat when $\alpha_T > 8000$.

Acknowledgement

The research was partly supported by the National Science Foundation under grant DMS-9006043 and DMS-9209129.

References

[1] Jaffrin, M. Y., Shapiro, A. H.: Peristaltic pumping. Annu. Rev. Fluid Mech. **3**, 13–36 (1971).
[2] Winet, H.: On the quantitative analysis of liquid flow in physiological tubes. Math. Research Center Technical Summary Report No. 2456, UW-Madison, 1982.
[3] Takabatake, S., Ayukawa, K.: Numerical study of two-dimensional peristaltic flows. J. Fluid Mech. **122**, 439–465 (1982).
[4] Takabatake, S., Ayukawa, K., Mori, A.: Peristaltic pumping in circular cylindrical tubes: a numerical study of fluid transport and its efficiency. J. Fluid Mech. **193**, 267–283 (1988).
[5] Hung, T. K., Brown, T. D.: Solid particle motion in two dimensional peristaltic flows. J. Fluid Mech. **73**, 77–96 (1976).
[6] Kaimal, M. R.: Peristaltic pumping of a Newtonian fluid with particles suspended in it at low Reynolds number under long wavelength approximations. Trans. ASME **45**, 32–36 (1978).
[7] Fauci, L. J.: Peristaltic pumping of solid particles. Comput. Fluids (to appear).
[8] Bestman, A. R.: Long wavelength peristaltic pumping in a heated tube at low Reynolds number. Dev. Mech. **10**, 195–199 (1979).
[9] Tang, D., Shen, M. C.: Peristaltic transport of a heat conducting fluid subject to Newton's cooling law at the boundary. Int. J. Eng. Sci. **27**, 809–825 (1989).
[10] Tang, D., Shen, M. C.: Numerical and asymptotic solutions for the peristaltic transport of a heat-conducting fluid. Acta Mech. **83**, 93–102 (1990).
[11] Joseph, D.: Stability of fluid motion II. New York: Springer 1976.
[12] Strikwerda, J. G.: Finite difference methods for the Stokes and Navier-Stokes equations. SIAM J. Sci. Statist. Comput. **5**, 56–58 (1984).
[13] Strikwerda, J. G., Nagel, Y. M.: A numerical method for the incompressible Navier-Stokes equations in three-dimensional cylindrical geometry. J. Comp. Phys. **78**, 64–78 (1988).
[14] Strikwerda, J. G., Nagel, Y. M.: Finite difference method for polar coordinate systems. ARO Report **87-1**, 1059–1076 (1987).

Author's address: D. Tang, Mathematical Sciences Department, Worcester Polytechnic Institute, Worcester, MA 01609, U.S.A.